Defect production in strained *p*-type $Si_{1-x}Ge_x$ by Er implantation

M. Mamor[a, b], B. Pipeleers[a], F. D. Auret[c] and A. Vantomme[a]

[a)] *Instituut voor Kern- en Stralingsfysica and INPAC, Katholieke Universiteit Leuven, Celestijnenlaan 200D, B-3001 Leuven, Belgium*

[b)]*Physics Department, Sultan Qaboos University ,P.O Box 50 Muscat 123 , Sultanate of Oman*

[c)] *Physics Department, University of Pretoria, Pretoria 0002, South Africa*

Strained *p*-$Si_{1-x}Ge_x$ (x = 5.3%, 10.2% and 15.4%) was irradiated at room temperature with 160 keV $^{166}Er^{2+}$ ions to a fluence of 1×10^{10} or 3×10^{13} Er/cm^2. The defects induced by ion implantation were investigated experimentally using high-resolution X-ray diffraction, Rutherford backscattering and channeling spectroscopy and deep level transient spectroscopy. X-ray diffraction indicates that the damage induced by Er implantation produces a slight perpendicular expansion of the SiGe lattice. For all compositions, channeling measurements reveal that Er implantation in *p*-$Si_{1-x}Ge_x$ to a fluence of 3×10^{13} Er/cm^2 induces an amorphous region below the $Si_{1-x}Ge_x$ surface. Annealing at 850°C for 30 s, results in a reduction in damage density, a relaxation of the implantation-induced perpendicular expansion of the SiGe lattice in the implanted region, while a more pronounced relaxation of the compressive strain SiGe is observed for higher Ge content (x = 0.10 and 0.15). On the other hand, for the annealed SiGe samples that were implanted with Er at the fluence of 10^{10} Er/cm^2, the compressive strain in the SiGe layer is nearly completely retained. Deep level transient spectroscopy studies indicate that two prominent defects with discrete energy levels above the valence band are introduced during Er implantation. Their activation energy was found to decrease with increasing Ge-content. However, the large local strain induced by high fluence Er implantation reduces the activation energy by 40 meV with respect to the low fluence Er implanted *p*-$Si_{1-x}Ge_x$. This shift (40 meV) in the activation energy remains constant regardless of the Ge content, suggesting that the $Si_{1-x}Ge_x$ layers remained fully strained after Er implantation. The observed defects are further compared to those introduced by alpha particle irradiation and electron beam metal deposition. The results indicate that defects introduced by Er implantation have similar electronic properties as those of defects detected after electron beam deposition and alpha particle irradiation. Therefore, it is concluded that these defects are due to the Er implantation-induced damage and not to the Er species specifically.

Electronic mail: mamor@squ.edu.om

I. Introduction

Erbium doped semiconductor materials exhibits stable luminescence in the near infrared (IR) region, at a wavelength of about 1.54 μm, which is nearly independent of the semiconductor host [1]. This specific wavelength corresponds to the minimum absorption window of optical fibers and is thus of great interest for optical communication technology. Previously, Si:Er visible light emitting diodes (LEDs) have been demonstrated [2]. Consequently, the optical activity of Er in Si has attracted special interest in association with potential applications of optical interconnects in Si chip technology [3-6]. One of the principal problems in the development of Er doped Si has been the strong quenching behavior of both the photo- and electroluminescence (EL) when in the range 77 K to room temperature [3, 5]. It has been observed that over this temperature range, the photoluminescence (PL) intensity decreases by over three orders of magnitude. However, significant effort has been devoted to the quest for Si based materials compatible with Si technology and able to act as light emitters. For instance, quantum confinement in Si quantum dots has been used as an efficient sensitizer for Er. Doing so, an increase of the effective absorption cross section of Er (10^{-14}-10^{-16} cm^2) by several orders of magnitude to that of Si (~ 10^{-21} cm^2) as well as an enhancement of the room temperature photoluminescence (PL) have been observed [7]. Recently, an enhancement of room temperature photololuminescence from Er-Ge co-doped SiO_2 has been also demonstrated [8]. Incorporation of Er in SiGe heterostructures and Si/SiGe quantum wells, either by implantation or during the growth of SiGe by molecular beam epitaxy, also allows an improvement of Er optical activity, due to the carrier confinement and optical confinement [9]. Moreover, the emission of Er doped SiGe was shown to be much more intense compared to Er doped silicon [9-11]. The enhancement of the Er luminescence depends strongly on the degree of strain in the SiGe host. The strain may modify the local environment around Er atoms and effectively improved the luminescent properties of Er [12, 13]. Room temperature 1.54 μm electroluminescence from Er doped $Si_{1-x}Ge_x$ light emitting diodes with germanium concentrations of 13% and 25% [14] and Er doped $Si/Si_{1-x}Ge_x$ waveguides with Ge concentrations x of 0%, 12%,

and 30% have been reported as well [15-16]. In this context, an important advantage of SiGe is that it can be easily integrated in the existing Si processing technology.

As is usually the case for semiconductor, ion implantation is the standard technique for selective doping device structures. The advantages of doping by means of ion implantation are the control of the concentration and the depth distribution of the dopants. However, a drawback of this technique is that the nuclear collisions occurring during ion implantation result in significant damage to the crystal lattice. Hence, for application in semiconductor devices, it is therefore important to study the lattice damage generated during the implantation process and its consequences on the electrical and structural properties of the material. The fundamental parameters determining the generation and recovery of defects during channeled and random implantation of high fluence Er implanted Si have been reported in detail [17-19]. Recently, progress has been made in the composition dependence and the effect of co-doped impurities on the thermal and structural properties of unstrained $Si_{1-x}Ge_x$ (x = 0.1 – 0.8) alloys implanted with Er^+ to a fluence of the order of 10^{15} cm^{-2} [20]. Touboltsev and Jalkanen [20] reported that post implantation annealing at different temperatures up to 600°C induces solid phase epitaxial regrowth leading to the recrystallization of the damaged SiGe matrix. However, although a few investigations on the electrical properties of deep level states in Er doped Si and on the structural properties of defects in Er doped unstrained $Si_{1-x}Ge_x$ have been published in the literature [4, 5], to our knowledge, there has been no report on electrically active deep levels in Er doped SiGe or on structural properties of defects in Er doped strained $Si_{1-x}Ge_x$.

In this paper, 160 keV erbium implanted in epitaxially grown *p*-$Si_{1-x}Ge_x$ samples has been investigated, both after implantation and after anneals designed to restore the sample crystallinity. In order to investigate the physical nature of the defects introduced by Er implantation, we have compared their electrical properties to those introduced during 5.4 MeV alpha particle irradiation, electron beam metal deposition and plasma etching. We also provided experimental evidence for the effect of the implantation-induced strain in *p*-$Si_{1-x}Ge_x$ on the electronic properties of implant-

related defects. In addition we report on the photoluminescence of $Si_{1-x}Ge_x$: Er prepared by ion implantation.

The paper is organized as follow: In Sec. II we present the growth process, the thickness and composition of our $Si_{1-x}Ge_x$ samples. The experimental conditions and the procedure that were used to implant the erbium as well as the different techniques used for the characterization of Er implanted $Si_{1-x}Ge_x$ samples are also presented in Sec II. Section III describes the results obtained from structural, electrical and optical characterization of the Er implanted $Si_{1-x}Ge_x$ films, and comprises a discussion. A comparison between the structural, electrical and optical properties will be also discussed in Sec III. In Sec IV, we summarize our paper.

II. Experimental

The $Si_{1-x}Ge_x$ layers studied here were grown by chemical vapor deposition (CVD). The deposition temperature was between 600 and 625 °C. A lightly boron doped ($4–6\times10^{16}$ cm^{-3}) Si buffer layer was first grown on the (100) p^+ silicon substrates. The epilayers of constant composition ($0 < x < 0.15$) are pseudomorphically strained: the thickness of the layers with a nominal Ge content of 5%, 10% and 15% is 380, 386 and 280 nm respectively, which is below the experimentally [21] and theoretically [22] calculated critical layer thickness (h_c). From high resolution X-ray diffraction (HRXRD) measurements, it was confirmed that there is no lattice relaxation in the as-grown p-$Si_{1-x}Ge_x$ epilayers. The structural properties and crystalline quality of the $Si_{1-x}Ge_x$ samples were investigated by HRXRD and Rutherford backscattering and channeling spectrometry (RBS/C). The RBS/C results yield a precise value for the actual Ge content in the layer as well as for the layer thickness. The experimental values of the Ge content in the respective $Si_{1-x}Ge_x$ layers are 5.3%, 10.2% and 15.4%, with a thickness of 380, 386 and 280 nm respectively. We conservatively estimated the error in Ge content to be 0.005. Channeling measurements indicate that all samples exhibit an excellent crystalline quality with a <100> channeling minimum yield of 3-4%.

Erbium-doped p-$Si_{1-x}Ge_x$ samples were obtained by implanting ^{166}Er at 300 K. The samples were tilted 10° away from the <001> axis to minimize channeling effects. The implantations were performed at 160 keV with a fluence of either 1×10^{10} or 3×10^{13} Er/cm^2,

referred to as low fluence (LF) and high fluence (HF), respectively. From the modeling tool Stopping and Range of Ions in Matter (SRIM) calculations the 160 keV Er ions are expected to have a projected range in the $Si_{0.898}Ge_{0.102}$ of R_p = 60 nm and a straggling σ = 41 nm, i.e. well-confined to the $Si_{0.898}Ge_{0.102}$ layer. Moreover, the above implantation energy was chosen so that the implanted regions of the $Si_{1-x}Ge_x$ samples were encompassed within the depletion regions occurring at the metal-$Si_{1-x}Ge_x$ Schottky contacts. A value of R_p (60 nm) and σ (41 nm) were found, more or less similar regardless of the investigated Ge content in the $Si_{1-x}Ge_x$ epilayers.

The strain present in the $Si_{1-x}Ge_x$ films was measured using HRXRD in θ-2θ geometry, using Cu-$K_{\alpha 1}$ radiation (λ = 1.54056 Å). One should consider two contributions to the strain, i.e., the strain in the pseudomorphic $Si_{1-x}Ge_x$ films due to the lattice mismatch between $Si_{1-x}Ge_x$ and Si (initial strain) and the additional elastic strain induced by the Er implantation (additional strain). The depth profile of the implantation-induced lattice damage was studied with RBS/C using a 1.57 MeV He^+ beam. The scattering angle of the detected particles was 105 degree. After implantation, a set of samples was annealed for 30 s at a temperature of 850°C in a rapid thermal annealing (RTA) set-up under a nitrogen flux.

For the electrical properties measurements, circular Ti contacts, 0.77 mm in diameter and 200 nm thick, were deposited onto the $Si_{1-x}Ge_x$ through a metal contact mask by electron beam evaporation (EB) with shielding the $Si_{1-x}Ge_x$ during the metal deposition from stray electrons. Subsequently the free-carrier concentration induced by boron doping of the epitaxial SiGe layers, as determined by capacitance voltage (C–V) measurements, was 8×10^{16}–1×10^{17} cm^{-3}.

The electrical properties of the erbium implantation-induced defects in the $Si_{1-x}Ge_x$ epilayers were studied by deep-level transient spectroscopy (DLTS) [23] using a lock-in amplifier (LIA) based system. The apparent activation energy (E_t) in the band gap and the apparent capture cross section (σ_a) of the defects were determined from Arrhenius plots of ln (T^2/e) versus 1/T where e is the emission rate at a temperature T. The DLTS measurements were recorded at a LIA frequency of 46 Hz, a quiescent reverse bias (V_r) of 1V and a filling pulse (V_p) of 1.6 V. We estimate error bars of ±10 meV for the absolute apparent activation measurements.

Photoluminescence measurements were performed at room temperature. The excitation of the samples is achieved by a Nd:Yttritium-aluminium-garnet laser operating at 532 nm via a 200

μm core optical fiber with a power density of ~5 Wcm^{-2}. The luminescence, collected by six surrounding fibers, is analyzed in a 0.25 m spectrometer with a liquid-nitrogen cooled InGaAs detector.

III. Results and discussion

A Structural characterization

Figure 1 shows the RBS/C spectra obtained from (a) the *p*- $Si_{0.898}Ge_{0.102}$ virgin sample, (b) the same sample after Er ions implantation with 160 keV to a fluence of 10^{10} cm^{-2} and (c) the same sample as in (b) subsequently annealed at 850°C for 30 s. It is clear that the aligned spectra of the as implanted and the annealed *p*- $Si_{0.898}Ge_{0.102}$ sample are only marginally higher than that obtained for the virgin sample.

The RBS/C spectra obtained from the virgin *p*- $Si_{0.898}Ge_{0.102}$ sample, after implantation to a fluence of 3×10^{13} Er/cm^2 and after annealing are shown in Fig. 2. The Er implantation produces a high damage peak below the surface where the channeling yield equals the random yield, indicating amorphization. Underneath this amorphous layer, end of range defects are observed in the aligned spectrum (energy range 0.7-0.9 MeV). Similar results were observed for the other Ge concentrations investigated in this study. After RTA, the defect density decreases, although not all damage could be removed from the SiGe layer, as indicated by the elevated channeling yield compared to the virgin sample. Further, we point out that post implantation annealing of the implanted $Si_{1-x}Ge_x$ ($x \neq 0$) alloy led to segregation of Er ions near the surface, as illustrated in Fig. 3. However, as can be seen from this figure, no channeling was observed for erbium, indicating that under these circumstances the Er ions do not occupy substitutional sites in the SiGe lattice.

Figure 4 shows the high-resolution (004) diffraction for the high fluence (~3×10^{13} cm^{-2}) as implanted $Si_{1-X}Ge_X$ samples for x = 0%, x = 5.3%, x = 10.2% and x = 15.4%. The diffraction pattern of Er implanted Si reveals the presence of irradiation-induced perpendicular strain as indicated by the low Bragg angle tail of the Si diffraction peak (see inset of Fig. 4). The defects introduced by Er implantation will generate a tensile perpendicular elastic strain in the implanted region, i.e. an increase of the perpendicular lattice parameter. To illustrate the latter behavior, Fig. 5

shows the HRXRD pattern from as grown (virgin), as implanted and post-implantation annealed SiGe (10.2% Ge) samples, both with HF (3×10^{13} cm^{-2}) and LF (1×10^{10} cm^{-2}). The relatively thick $Si_{1-x}Ge_x$ layers ~280 nm yield narrow XRD peaks, resulting in an estimated uncertainty in the perpendicular lattice constant of ± 0.001 Å.

A satellite peak arises at the low angle side of the $Si_{0898}Ge_{0.102}$ (004) reflection due to the local expansion of the $Si_{0898}Ge_{0.102}$ lattice in the implanted area, caused by the implantation induced defects. Similar to the case of ion implantation into other semiconductors, the lattice strain and damage in the $Si_{0898}Ge_{0.102}$ crystal are expected to exhibit the same depth distribution [14-16]. A more pronounced tail appears for high fluence as compared to the low Er fluence. With increasing fluence, i.e., increasing defect concentration, the lattice expansion increases accordingly, hence the tail of satellite peak shifts towards lower angles and at the same time its intensity decreases and gradual amorphisation of the $Si_{1-x}Ge_x$ lattice at higher fluence (3×10^{13} cm^{-2}). This tail actually is a distribution of a strain profile which is correlated to the defect distribution – both profiles exhibit the same shape. Since the strain is caused by the defect distribution, the maximum induced strain (corresponding to the extreme minimum Bragg angle of this tail) is taken as a measure to quantify the implantation-induced elastic strain. Because of the highly disorder layer for HF Er implantation as confirmed from RBS/C, the minimum angle from the HRXRD spectra was determined at a fixed intensity level above the background and accordingly, the maximum perpendicular strain ($\Delta b_\perp/b_\perp$) for HF was deduced as 3.4×10^{-3}, where $b_\perp$ is the perpendicular lattice parameter and $\Delta b_\perp$ is difference in $b_\perp$ between HF and LF. The HRXRD spectrum obtained from a high Er fluence implanted sample followed by RTA annealing at 850°C for 30 indicates that due to the post-implantation annealing, strain relaxation is observed compared to the virgin $Si_{0.898}Ge_{0.102}$ sample. Similar results with a small variation of the lattice expansion were observed in the HRXRD spectra of implanted/annealed sample with low Er fluence (LF) (~1×10^{10} cm^{-2}) and indicates that as expected, the lattice expansion increases with increasing the fluence ($1 \times 10^{10} - 3 \times 10^{13}$ cm^{-2}),

since a higher fluence induces more damage and consequently a larger perpendicular strain. At low Er fluence, we have observed only a marginally higher aligned RBS spectra as compared to that observed for the virgin sample (see Fig. 1). As a result, we could not observe a pronounced tail as in the case of HF. Furthermore Fig. 5 shows also that Er implantation-induced perpendicular strain in the $Si_{0898}Ge_{0.102}$ exhibits a small shift of the main $Si_{0.898}Ge_{0.102}$ XRD diffraction peak to lower Bragg angle with increasing Er fluence. The Si substrate diffraction peak is not affected by the implantation, as expected since the defect profile is confined to the $Si_{1-X}Ge_{X}$ epi-layer. We believe that the small shift of the main $Si_{0.898}Ge_{0.102}$ XRD peak is due to the total average strain because of relatively thin $Si_{1-x}Ge_{x}$. This total average strain corresponds to the average of the induced and the pseudomorphic strain due to Ge content. Similar results have been found in our $Si_{1-x}Ge_{x}$ samples for all Ge contents. The above results indicate that the implantation-induced strain is the same for the different $Si_{1-x}Ge_{x}$ films having different initial values of strain due to different Ge content. This additional strain is not affected by the initial value of strain in the unimplanted pseudomorphic $Si_{1-x}Ge_{x}$ films. This fact strongly suggests that the Er ions implantation with a given fluence produces the same additional strain regardless the concentration of Ge. This result is consistent with that reported earlier in Ref [24] which state that the initially uniform strain of the $Si_{1-x}Ge_{x}$ films does not affect the implantation-induced strain generated by Si irradiation.

In Fig. 6, we have plotted the theoretical perpendicular lattice parameter according to Vegard's law for both fully strained and fully relaxed $Si_{1-x}Ge_{x}$ alloy (solid lines). The Poisson ratio used to extract the theoretical perpendicular lattice constants for $Si_{1-x}Ge_{x}$ films is calculated by using a linear dependence on Ge-content, where the Poisson ratio at 300 K for Si and Ge are 0.28 and 0.26, respectively [25]. In addition, the experimentally measured perpendicular $Si_{1-x}Ge_{x}$ lattice parameter ($0 \leq \times \leq 0.15$) is also shown for the as implanted samples at two different fluences (1×10^{10} and 3×10^{13} cm^{-2}) and for post-annealed samples. This figure indicates that after annealing, no strain relaxation occurs in the $Si_{1-x}Ge_{x}$ samples for the low fluence (1×10^{10} cm^{-2}) Er-implantation, except for the highest Ge concentration (x = 0.154), where within the experimental

error, only a minute relaxation of the SiGe epilayer is observed, while for high fluence (3×10^{13} cm^{-2}) Er-implantation, RTA induces a significant strain relaxation for higher Ge content (10.2 and 15.4 % Ge). The reason for this behavior is that the high fluence implant induces a larger defect concentration in the $Si_{1-x}Ge_x$ layer, the subsequent annealing causes diffusion and segregation of the defects at the interface causing the compressive strain relaxation. The fact that the elastic strain is retained after low fluence implantation in $Si_{1-x}Ge_x$ ($0 < x < 0.15$) and subsequent RTA is an important issue when implementing low fluence Er implantation in strained SiGe based device processing. Moreover, it is also clear from Fig. 6 that for a given Ge content, low fluence Er implantation results in a small change in perpendicular lattice constant with respect to high fluence Er implantation, as revealed by the smaller shift of the main diffraction peak (see Fig. 5). This small shift observed in Fig. 5 between the main peak of high and low Er fluence implanted $Si_{0.898}Ge_{0.102}$ induces a difference in average strain of about 1.7×10^{-3}.

Through the comparison of the compositional dependence, the effect of the fluence and the post-implantation annealing, the following conclusions can be drawn. For a given Ge content, HRXRD results indicate that the lattice expansion increases with increasing fluence ($1 \times10^{10} - 3 \times 10^{13}$ cm^{-2}) since higher fluence Er implantation induces more damage and consequently a larger perpendicular strain. A variation of the total average strain of 0.6×10^{-4} between the low and high Er fluence is estimated from the shift of the main SiGe peak. On the other hand, the maximum elastic strain in the HF Er implanted region extracted from the minimum angle in the HRXRD spectra was determined to be 3.4×10^{-3}. RTA at 850 °C for 30 s results in a decrease of the induced damage, since the defects become mobile in the crystal and can recombine, resulting in a reduction of the perpendicular strain. Note that a drastic relaxation of the compressive strain of about 80% is observed for $Si_{1-x}Ge_x$ with higher Ge content (10.2 and 15.4 % Ge) after post-implantation annealing of HF Er implantation. The full width at half maximum of $Si_{1-x}Ge_x$ (10.2 and 15.4 %Ge) diffraction peak after RTA is broadened, which can either correspond to an increase of threading dislocation density or to a gradual strain profile after post-implantation annealing.

An attempt will be made to correlate the structural properties of defects and strain as determined by RBC/C and HRXRD to the electrical properties determined by the DLTS measurement in the following section.

B Electrical characterization

Figure 7 depicts the DLTS spectra obtained from 160 keV Er implanted *p*-type $Si_{1-x}Ge_x$ to a fluence of 1×10^{10} ions/cm^2. The DLTS spectrum from the unimplanted samples (not shown here) indicated that no defects with peaks between 40K and 300K are present in detectable concentrations. For all investigated compositions, erbium implantation into *p*-$Si_{1-x}Ge_x$ introduces two prominent defects (HEr2 and HEr3) in the band gap of *p*-$Si_{1-x}Ge_x$. The defect labeling in this study is according to the following convention: for example HEr2, (H) indicates a hole defect, Er implies that it was introduced during erbium implantation and (2) indicates the second defect starting from the high temperature side of the DLTS scan. Furthermore, the DLTS spectra in Fig. 7 show that the peak temperatures of the HEr2 and HEr3 defects shift towards lower temperature with increasing Ge content, which is associated with a decrease in the semiconductor band gap with increasing Ge-content. A comparison of the variation of the activation energies to the change in the band gap indicates the trend shown in Table I. Within the experimental uncertainty, the composition-related change in the activation energies of the two defects is virtually the same as the corresponding variation in the band gap for a change in x from 0.053 to 0.154 (i.e. from 1.07 eV to 0.987 eV). Taking into account that the band gap variation in $Si_{1-x}Ge_x$/Si heterojunction is contained mainly in the valence band [26], the HEr2 and HEr3 defects detected in SiGe with 5.3% Ge are the same as those detected in SiGe with 10.2% and 15.4% Ge and are pinned to the conduction band. The energy level of HEr1 observed only in materials with high Ge content (x = 10.2 and 15.4%) shows a much smaller variation with Ge content compared to the HEr2 and HEr3 defects. Since HEr1 is only observed in $Si_{1-x}Ge_x$ samples with higher Ge content, it could be a Ge-related defect introduced by Er implantation.

In order to elucidate the origin of the defect levels, the DLTS spectra of the Er implanted $Si_{1-x}Ge_x$ were compared to those obtained for other irradiation conditions. Figure 8 compares the defects created in $Si_{0.947}Ge_{0.053}$ (a) by Er implantation, (b) after electron beam deposition (EBD) of Scandium (no shielding of secondary electrons) [27], and (c) by 5.4 MeV alpha particle irradiation

[27]. The electron fluence on the $Si_{1-x}Ge_x$ sample was estimated by measuring the current through the sample holder during EBD. It is quite obvious that the two major defects HEr2 and HEr3 detected after Er implantation are similar to He2 and He3 detected after EBD and Hal2 and Hal3 detected after alpha particle irradiation, respectively. In Fig. 9, we show the variation of the defect activation energy as a function of the Ge content for Er implanted *p*-$Si_{1-x}Ge_x$, along with the measured activation energy of the main defects in EBD and alpha particle-irradiated *p*-$Si_{0.947}Ge_{0.053}$. This comparative study of E_T variation clearly demonstrate a good similarity between the three different processes. This comparison demonstrates that these defects are not Er-related but solely related to implantation-induced damage and primary defects.

To explain why EBD creates similar defects compared to 5.4 MeV alpha particles and Er implantation, the mass and energy of these ions have to be considered. Unlike MeV He ions, the e-beam evaporators utilize electrons with energies of between 2 and 20 keV to melt the metal. It is generally believed that defects introduced during EBD of metal Schottky contacts are due to ionized residual vacuum gases generated by collision between the gas particles and the electron beam in the EBD chamber. The defects can also be caused by heavier positive ion of the metal, because of the negative accumulated charges at the surface of the substrate [28]. It has also shown that when the electrons strike the molten metal, X rays of various energies and intensities are produced. During evaporation, these X rays will irradiate the substrate on which the metal is deposited [28]. These X rays are intense enough to induce defects in the *p*-$Si_{1-x}Ge_x$ films. Apart from the X rays, stray electrons from the filament (the primary source of high energy electrons), as well as electrons backscattered from the molten metal target and elsewhere in the vacuum chamber, will also reach the *p*-$Si_{1-x}Ge_x$ substrate [28]. Following the above arguments, it is worthwhile noting that EBD produced similar defects as those introduced by Er implantation and alpha particle irradiation. The physical structure of the defects is independent of implanted species and strongly depends on the mass and amount of energy deposited through elastic recoils.

To further confirm that the defects introduced by Er implantation are not Er-related defects, DLTS depth profiling was performed by recording spectra at fixed V_r but incrementing V_p in small

steps from one scan to the next. The approach of Zhota *et al*. [29] was used to obtain the defect concentration as a function of depth below the surface. Figure 10 illustrates the depth profiles of the major defect (HEr2) detected in p-$Si_{0.947}Ge_{0.053}$ after Er implantation and defect He2 observed after e-beam deposition which is believed to be the same defect as HEr2. Both depth profiles have a similar shape but different concentrations. The defect HEr2 has a maximum concentration of 7.8×10^{14} cm^{-3} at a depth of 66 nm and is observed to extend 150 nm below the surface, while He2 has a maximum concentration of 7×10^{15} cm^{-3} at 50 nm below the surface. Because 160 keV Er penetrates the $Si_{1-x}Ge_x$ to 60 nm below the surface, it is believed that interstitials and vacancies created in this damaged "near surface" region diffuse into the material forming pairs and complexes. However, the defects introduced after Er implantation have a lower defect concentration, which is due to the lower implantation fluence (1×10^{10} Er/cm^2). Moreover, both depth profiles of HEr2 and He2 are in good agreement with the SRIM simulated vacancy profile (Fig. 10). This comparison further supports that the defects introduced by Er implantation are not related to Er but only to implantation-induced damage.

In previous work [30] we have showed that increasing the Ge content led to a decrease in the activation energy of the defect He2 and this decrease followed the same trend as the band-gap variation, suggesting that this defect detected in p-$Si_{1-x}Ge_x$ is the same as that observed in p-Si. Taking the band gap change into account and assuming that the majority of the band gap change is taken up in the valence band [26], it was speculated that the defects HEr2 and HEr3 detected in material with 5.3%, 10.2% and 15.4% should be the same as those detected in p-Si. By considering the composition related change in the activation energy of the deep levels to be similar in size to the change of strained band gap $Si_{1-x}Ge_x$, the defect Her2 and Her3 should be detected in p-type Si at 0.54±0.01 eV and 0.36 ±0.01 eV above the valence band, respectively. We have considered for example the band gap in pseudomorphic $Si_{1-x}Ge_x$ is changed by ~0.045 eV from 1.12 eV for x = 0 to 1.075 eV for x = 0.05 [31]. Recently, several groups reported on a deep level center with a level E_v + 0.53 eV in irradiated boron silicon [32, 33]. The center labeled H3 (0.535) and H (052) were

shown to be B_i–B_s–H formed by the capture of B_i at a hydrogen passivated B_s site. The extracted activation energy of HEr3 in p-type Si (E_v+0.36 eV) is the same as a defect detected in Czochralski-grown p-Si after plasma etching and the level has been assigned to be C_i-O_i (34). Following the above arguments, the defects HEr2 and HEr3 detected in Er implanted p-type $Si_{1-x}Ge_x$ are tentatively attributed to be B_i–B_s–H and C_i-O_i centers, respectively.

In order to investigate the electronic properties of the defects introduced into p-$Si_{1-x}Ge_x$ by high fluence Er implantation and to acquire information on the influence of the induced strain on the induced defects, DLTS measurements were also conducted on $Si_{1-x}Ge_x$samples irradiated with high Er fluence, both after implantation and after annealing at 850 °C for 30 s. Figure 11 shows the DLTS spectra taken from p-$Si_{1-x}Ge_x$, with x = 0.053, 0.102, and 0.154, implanted at 160 keV Er ions to a fluence of 3×10^{13} cm^{-2}. The Er implanted p-$Si_{1-x}Ge_x$ introduces a prominent hole trap, HEr2a, HEr2b and HEr2c, detected in p-$Si_{1-x}Ge_x$ with x = 0.053, 0.102 and 0.154, respectively. Since the samples have been grown under the same conditions with the same doping concentration and also have been irradiated under the same conditions, defects HEr2a, HEr2b and HEr2c, are expected to be related to the same defect, which we label as HEr in the discussion below. The temperature peak of the HEr defect shifts towards lower temperature with increasing Ge content, most likely because of the decrease of the $Si_{1-x}Ge_x$ band gap with increasing Ge content. Here again, as in the case of low fluence Er implanted p-$Si_{1-x}Ge_x$, the energy position changes of HEr are closely related to the band gap changes in strained $Si_{1-x}Ge_x$ epilayers [31, 35]. For comparative purpose, the inset of Fig. 11 shows examples of DLTS spectra taken from p-$Si_{0.898}Ge_{0.102}$ samples implanted with high (3×10^{13} cm^{-2}) and low Er fluence (1×10^{10} cm^{-2}) as well as the high fluence post-annealed sample. From this comparison, it is clear that the DLTS peak HEr introduced after high fluence Er implantation is shifted to lower temperature compared to the defect HEr2 detected after low Er fluence implantation with an increase in the peak intensity under identical DLTS conditions. After RTA the DLTS peak shifts to higher temperature compared to the as implanted sample with the same Er fluence. This trend again follows the same increase (decrease) of the band gap of $Si_{1-x}Ge_x$ with increasing (decreasing) induced strain. Similar results were observed all Ge contents investigated in this work. After annealing, a broadening of HEr1 is observed, due to the strain relaxation, which is consistent with our HRXRD results.

Using low electric field conditions [V_r=0.5V, V_p=0.5V], we determined the activation energy and apparent capture cross section of HEr1. Figure 12 shows the Arrhenius plots of the main defects detected in the low fluence and high fluence Er implanted p-$Si_{1-x}Ge_{x}$, samples with various Ge contents. The signatures of the defects are summarized in Table I. From Fig. 12 and Table I, where we compare the DLTS signature of defects introduced after high and low fluence implantation as well as after annealing, one can summarize and interpret the above results as follow:

- First: for high Er fluence implantation (3×10^{13} cm^{-2}) the composition related change in the activation energies of HEr is virtually the same as the corresponding change in the band gap of the strained $Si_{1-x}Ge_x$ and indicates that such level is pinned with respect to the conduction band.
- Second, for a given Ge content, it seems that the induced strain results in a red shift of the activation energy. From SRIM, the calculated ion profiles show a Gaussian Er distribution with a projected range of 60 nm. Since the additional strain is caused by the defect distribution, the maximum defect concentration and consequently the maximum strain is localized close to the surface, i.e. embedded in the depletion layer and hence within the region probed by DLTS.

As already mentioned before, the maximum value of implantation-induced strain in the SiGe samples implanted with higher Er fluence is higher than that of low fluence and this additional value of strain is the same for all Ge content. This different strain value results in a reduction of the band gap of the epitaxial SiGe material [35]. For instance, the defect HEr (0.45 ± 0.01 eV) and HEr2 (0.49 ± 0.01 eV) observed in high and low fluence Er implanted p-$Si_{0.947}Ge_{0.053}$ respectively, are the same. However, we have observed the same shift (by ~35 ± 10 meV) for all compositions investigated in this study. One can conclude from the constant (as a function of Ge content) difference of activation energy between the defect introduced in low fluence and high fluence Er implantation, that (i) the p-$Si_{1-x}Ge_x$ is still fully strained and that (ii) the induced strain by Er implantation does not modify the pseudomorphic strain in the epilayer materials. This finding is consistent with the above HR-XRD results where we demonstrated that either using low or high Er^+ implantation the p-$Si_{1-x}Ge_x$ remains fully strained. An important issue is to determine the difference

in the total induced strain responsible for the shift in the activation energy between the low fluence and high fluence Er implanted $Si_{1-x}Ge_x$. However, if the $Si_{1-x}Ge_x$ is biaxially compressed, the band gap of $Si_{1-x}Ge_x$ is reduced by ~117 meV per percent biaxial compressive strain [26, 36]. The lattice constant of $Si_{0.898}Ge_{0.102}$ is about 0.42% larger than that of Si, thus fully strained $Si_{0.9}Ge_{0.1}$ has a band gap of ~ 50 meV smaller than that of fully relaxed $Si_{0.892}Ge_{0.102}$ [31]. According to the decrease of the band gap of pseudomorphic $Si_{1-x}Ge_x$ with increasing strain by increasing Ge content [31, 35], and the fact that the shift is almost independent of the Ge content, the shift for a given Ge content of about ~35 meV corresponds to a change in biaxial strain in the $Si_{1-x}Ge_x$ film of 2.94×10^{-3}. This result indicates that Er^+ implantation-induced perpendicular elastic strain in the pseudomorphic $Si_{1-x}Ge_x$ lattice and leads to $\Delta E_a/\Delta\varepsilon \approx -11.9$ eV/unit strain, where ΔE_a and $\Delta\varepsilon$ are the difference in the activation energy and the change of strain, respectively. Interestingly, this strain value of about 2.94×10^{-3} agrees with the above mentioned difference of the maximum strain value (3.4×10^{-3}) between HF and LF Er implanted $Si_{1-x}Ge_x$ as determined from HRXRD. This is slightly larger than the value of 1.6×10^{-3} determined from the shift of the main XRD peak between HF and LF Er implanted $Si_{1-x}Ge_x$ for a given Ge content. It must be noted that the strain value of the epitaxial layer varies as we go from the surface into the bulk of $Si_{1-x}Ge_x$ (i.e. the local implantation-induced strain is biggest near the maximum distribution of defect and smallest outside. The value $(0.5\text{-}0.6) \times 10^{-4}$ which is the strain difference between the low and high Er fluence is therefore an average value, and the strain in the depth region studied by DLTS could be very different from this average value.

We now investigate the influence of RTA of Er implanted p-$Si_{1-x}Ge_x$. Curve (c) of the inset of Fig. 11 taken from high fluence Er implanted p-$Si_{0.898}Ge_{0.102}$ clearly illustrates a broadening of the DLTS peak and an asymmetric DLTS peak shape. From HR-XRD, we have shown that after RTA of the high fluence Er implanted p-$Si_{1-x}Ge_x$ (x =0.102 and 0.154), the epilayers are partly relaxed. It can be expected that relaxation is accompanied by the generation of threading dislocations within the SiGe layer [37] and clusters and extended defects can be created [38]. Since

these defects overlap in the DLTS spectra, it is difficult to resolve the positions of these peaks accurately.

C. Optical characterization

Figure 13 shows the photoluminescence spectra measured at 300 K for all $Si_{1-x}Ge_x$ samples ($0 \leq x \leq 0.154$) implanted with 3×10^{13} Er/cm^{-2} followed by RTA at 850 °C for 30 s. The spectra consist of a dominant sharp line at 1.542 µm accompanied by some high-energy features. It is generally assumed that the dominant sharp line at about 1.54 µm is the transition from the lowest $^4I_{13/2}$ state to the lowest ground state of $^4I_{15/2}$. Neither the Ge content nor the strain influences the peak position and the emission intensity of these samples.

IV. Summary

Erbium implantation-induced defects in strained, epitaxial *p*-type $Si_{1-x}Ge_x$ layers have been investigated by HRXRD, RBS/C and DLTS. From HRXRD measurements, we have demonstrated that the implantation-induced defects generate a slight expansion of the SiGe lattice in the implanted region and the induced strain is the same for the different $Si_{1-x}Ge_x$ films having different initial strain values due to their different Ge content. (x= 5.3%, 10.2% and 15.4%). Annealing of the samples implanted to a fluence of 10^{10} Er/cm^2 for 30 s at 850°C, leads to a relaxation of the implantation-induced strain, retaining the initial pseudomorphic strain. In contrast, annealing of the SiGe samples implanted with Er to a fluence of 3×10^{13} Er/cm^2 leads to a relaxation of the pseudomorphic strain, a relaxation which is more pronounced for higher Ge content (x =0.102 and 0.154).

RBC/C measurements revealed that high defect concentrations are created below the surface by implantation of 3 x 10^{13} Er/cm^2 and show the formation of an amorphous layer regardless the Ge content under investigation. Annealing of the samples for 30 s at 850°C, leads to reduction of the implantation-induced damage in SiGe epi-layers.

DLTS measurements confirmed that that erbium-implanted *p*-$Si_{1-x}Ge_x$ epilayers introduced two prominent defects with discrete energy levels for all x values. The two major defects HEr2 and HEr3 have an activation energy which changes with increasing Ge content according to the band

gap variation of the SiGe, indicating that the defects HEr2 and HEr3 are pinned to the conduction band, while the HEr1 defect is pinned to the valence band.

From a comparison of the DLTS "signatures" of Er implanted samples to those of e-beam deposition, argon plasma etching and alpha particle irradiation of the same material, it is shown that the defects introduced by Er implantation are similar to those introduced by alpha particle irradiation and electron beam metal deposition. This result indicates that the defects introduced by Er implantation are related primarily to implantation-induced damage and Frenkel pairs which are mobile at room temperature to form stable defects such as point defects (i.e. vacancies and interstitials).

From a comparison of the electronic properties of defects introduced after high and low fluence Er implanted p-$Si_{1-x}Ge_x$ and after annealing, it was demonstrated that the strain induced by Er implantation reduces the activation energy in the as-implanted p-$Si_{1-x}Ge_x$. The shift in the activation energy remains constant regardless of the Ge content, suggesting that the $Si_{1-x}Ge_x$ layers were fully strained before and after implantation. After annealing of the samples for 30 s, a broadening of HEr1 DLTS peak is observed and its position is shifted to higher temperature compared to the as- implanted p-$Si_{1-x}Ge_x$. This is possibly due to an increase of the activation energy with increasing strain relaxation.

The photoluminescence properties of the implanted Er into $Si_{1-x}Ge_x$ demonstrate that the spectra consist of a dominant sharp line at 1.542 μm and some high-energy features. Neither the intensity of the Er emission from the samples nor the emission peak position were influenced by the Ge content or the strain in the epilayers.

The authors acknowledge the Fund for Scientific Research Flanders (FWO), the financial support from the Inter-University Attraction Pole (IUAP P6/42) and the KULeuven (GOA/09/006 and INPAC). Thanks also to J. Maes from Laboratorium voor Vaste-Stoffysica en Magnetisme, Katholieke Universiteit Leuven, Belgium for the photoluminescence measurements.

References

[1] Rare Earth Doped Semiconductors II, edited by S. Coffa, A. Polman, and R.N. Schwartz, Mater. Res. Soc. Symp. Proc. **422**, (1996).

[2] H. Ennen, G. Pomrenke, A. Axmann, K. Eisele, W. Haydl and J. Schneider, Appl. Phys. Lett. **46** (1985), 381.

[3] J. Michel, J.L. Benton, R.F. Ferrante, D.C. Jacobson, D.J. Eaglesham, E.A. Fitzgerald, Y.H. Xie, J.M. Poate and L.C. Kimerling, J. Appl. Phys. **70** (1991), 2672.

[4] J.L. Benton, J. Michel, L.C. Kimerling, D.C. Jacobson, Y.H Xie, D.J. Eaglesham and J.M. Poate, J. Appl. Phys. **70** (1991), 2667.

[5] S. Coffa, G. Franzo, F. Priolo, A. Polman and R. Serna, Phys. Rev. B**49** (1994), 16313, S. Libertino, S. Coffa, G. Franzo and F. Priolo, J. Appl. Phys. **78** (1995), 3867.

[6] H. Przybylinska, W. Jantsch, Yu. Suprun-Belevitch, M. Stepikhova, L. Palmetshofer, G. Hendorfer, A. Kozanecki, R.J. Wilson and B.J. Sealy, Phys. Rev. B**54** (1996), 2532.

[7] F. Priolo, G. Franzo, D. Pacifici, V. Vinciguerra, F. Lacona, and A. Irrera, J.Appl. Phys. **89** (2001), 264.

[8] C.L. Heng, T.G. Finstad, P. Storas, Y.J. Li, A.E. Gunnaes and O. Nilsen, Appl. Phys. Lett. **85** (2004), 4475.

[9] M.Q. Huda, J. H. Evans-Freeman, A. R. Peaker, D. C Houghton, B. Joyce, A. Nejim, J. Vac. Sci. Tech B**16** (1998), 2928,. M. Q. Huda, A. R. Peaker, J. H. Evans-Freeman, D. C. Houghton and W. P. Gillin Electronics Letters, **33** (1997), 1182.

[10] M. Q. Huda and A. R. Peaker, Solid State Electronics, **45** (2001), 1927.

[11]. K. D. Vernon-Parry, I. D. Hawkins, J. H. Evans-Freeman, P. Dawson and A. R. Peaker, Materials Science and Engineering. **81** (2001), 164.

[12] T. Ishiyama, S. Nawae, T. Komai, Y. Yamashita, Y. Kamiura, T. Hasegawa, K. Inoue, and K. Okuno, J. Appl. Phys. **92** (2002) 3615.

[13] T. Ishiyama, S.Yoneyama,Y.Yamashita,Y. Kamiura,T. Date,T. Hasegawa, K. Inoue, K. Okuno, Physica B **376–377** (2006) 122.

[14] A. T. Naveed, ,J.H. Evans-Freeman, K.D. Vernon-Parry, A. C. Wright, D. C. Houghton, andA.R. Peaker, Semicond. Sci. Technol. **15** (2000) 91

[15] S. J. Chang, D. K. Nayak, Y. Shiraki, J. Appl. Phys. **83** (1998), 1426.

[16] E. Neufeld, A. Sticht, A. Luigart, K. Bruner, G. Abstreiter, Appl. Phys. Lett. **73** (1998), 3061.

[17] M.F. Wu, A. Vantomme, H. Pattyn, G. Langouche and H. Bender, Appl. Phys. Lett. **68** (1996), 3260

[18] A. Vantomme, M.F. Wu, U. Wahl, J. De Wachter, S. Degroote, H. Pattyn, G. Langouche and H. Bender, Nucl. Instr. Meth. B**120** (1996), 190.

[19] S.M. Hogg, B. Pipeleers; A. Vantomme, M. Swart, Appl. Phys. Lett. **80** (2002), 4363.

[20] V. Toubolstev and P. Jalkanen, J. Appl. Phys. **97** (2005), 013526.

[21] R. People and J.C. Bean, Appl. Phys. Lett. **47** (1985), 322.

[22] D. C. Houghton, J. Appl. Phys. **70** (1991), 2136.

[23] D.V. Lang, J. Appl. Phys. **45** (1974), 3014.

[24] D. Y. C. Lie, A. Vantomme, F. Eisen, T. Vreeland, M. A Nicolet, T. K. Carns, V. Arbet-Engels and K. L. Wang, J. Appl. Phys. **74** (1993), 6039.

[25] J. J. Wortman and R.A. Evans, *J. Appl. Phys.* **36** , (1965), 153.

[26] C. G. Van de Walle and R. M. Martin Phys. Rev. B **34** (1986), 5621.

[27] M. Mamor, F. D. Auret, M. Willander S.A. Goodman, G. Myburg, and F. Meyer, *Semicond. Sci. Technol.* **14** (1999), 611.

[28] P. K. Bhattacharva, A. Reisman, and M. C. Chen, J. Electron. Mater. **17**, 273 (1988).

[29] Y. Zohta and M. O. Watanabe, J. Appl. Phys. **53** (1982), 1809.

[30] M. Mamor, F. D. Auret, S. A. Goodman, and G. Myburg, Appl. Phys. Lett. **72** (1998), 1069.

[31] D. Dutartre, G. Bremond, A. Souifi and T. Benyattou, Phys. Rev. B **44** (1991), 11525.

[32] N. Yarykin, O. V. Feklisova and J. Weber, Phys. Rev. B **69** (2004), 045201.

[33] F. Volpi and A. R. Peaker, I. Berbezier and A. Ronda, J. Appl. Phys. **95** (2004), 4752.

[34] O. O. Awadelkarim, T. Gu, P. I. Mikulan, R. A. Ditizio, S. J. Fonash, K. A. Reinhardt, and Y. D. Chan, Appl. Phys. Lett. **62** (1993), 958.

[35] D. V. Lang, R. People, J. C. Bean and A. M. Sergent, Appl. Phys. Lett. **47** (1985), 1333.

[36] A. St. Amour, C. W. Liu and J. C. Sturm, Appl. Phys. Lett. **67** (1995), 3915.

[37] A. R. Powell, S.S. Iyer and F. K. LeGoues, Appl. Phys. Lett. **64** (1994), 1856.

[38] S. A. Ringel and P. N. Grillot, in Semiconductor and Semimetals, edited by R. Hull and J. C. Bean (1999), Vol 56, p.293.

TABLE I. Electronic properties of the prominent HEr2 (a-c), the minor hole traps HEr3 (a-c) and HEr (1-3) detected by DLTS in 160 keV Erbium implanted epitaxially grown p-$Si_{1-x}Ge_x$/Si at low Er fluence (1×10^{10} Er/cm^2) and high fluence Er (3×10^{13} Er/cm^2), respectively.

Defect label	*Ge content*	E_t *(eV)*	σ_a *(cm^2)*	T_{peak} [(a)] *(K)*
Low fluence (1×10^{10}Er/cm^2)				
Her1				
HEr2	0.053	0.49	1.7×10^{-13}	221
HEr3	0.053	0.31	1.2×10^{-15}	177
HEr2	0.102	0.41	3.5×10^{-14}	199
HEr3	0.102	0.24	9.3×10^{-17}	160
HEr2	0.154	0.35	2.2×10^{-14}	182
HEr3	0.154	0.20	2.7×10^{-17}	145
High fluence (3×10^{13}Er/cm^2)				
HEr2a	0.053	0.45	1.8×10^{-13}	195
HEr2b	0.102	0.37	3.4×10^{-14}	180
HEr2c	0.154	0.32	2.1×10^{-14}	162

[(a)] Peak temperature at a lock-in amplifier frequency of 46 Hz, i.e. a decay time constant of 9.23 ms.

FIGURE CAPTIONS

FIG. 1. (Color online) Random and <001> aligned RBS spectra for 1×10^{10} cm^{-2} Er (160 keV) as-implanted $Si_{0.90}Ge_{0.10}$ samples and after RTA (850 ºC, 30 s). The spectrum of the virgin $Si_{0.898}Ge_{0.102}$sample in channeling mode is also depicted.

FIG. 2. (Color online) Random and <001> aligned spectra for 3×10^{13} cm^{-2} Er (160 keV) as-implanted $Si_{0.90}Ge_{0.10}$ samples and after RTA (850 ºC, 30 s). The spectrum of the virgin $Si_{0.9}Ge_{0.1}$sample in channeling mode is also depicted.

FIG. 3. (Color online) The Er part of the RBS spectra after RTA (850 ºC, 30 s) of Er implanted $Si_{0.898}Ge_{0.102}$at 160 keV to a fluence of 3×10^{13} cm^{-2}. The RBS spectra after RTA of Er implanted silicon at 160 keV to a fluence of 3×10^{13} cm^{-2} is also shown for comparison.

FIG. 4**.** (Color online) High-resolution X-ray θ-2θ (004) diffraction of *p*-$Si_{1-x}Ge_x$ (a) after 160 keV Er implantation with 3×10^{13} Er/cm^2, and (b) the same sample after RTA of 850 ºC for 30 s. For comparison, the HRXRD diffraction from virgin Si, as implanted and after post implantation annealing is shown in the inset.

FIG5. (Color online) High-resolution X-ray θ-2θ (004) diffraction of the *p*-$Si_{0.898}Ge_{0.102}$ from a virgin sample, as implanted to a fluence of 1×10^{10} cm^{-2} or 3×10^{13} cm^{-2} as well as after post-implantation annealing.

FIG. 6**.** Perpendicular lattice parameter extracted from HRXRD measurements for $Si_{1-x}Ge_x$: Er as-implanted and after RTA (850 ºC, 30 s). The solid lines indicate the theoretical perpendicular lattice parameter for both fully strained and fully relaxed $Si_{1-x}Ge_x$ epilayers.

FiG. 7. DLTS spectra of 1×10^{10} cm^{-2} 160 keV Er implanted *p*-SiGe with different Ge-content. The spectra were recorded at a LIA frequency of 46 Hz.

FIG. 8. DLTS spectra of p-$Si_{0.947}Ge_{0.053}$ after 160 keV Er implantation (fluence = 1×10^{10} cm^{-2}) (a), after e-beam deposition with no shielding (b) and after 5.4 MeV alpha particle irradiation (c).

FIG. 9. Variation of the defect activation energy E_T(x) of Er implantation at 160 keV to a fluence of 1×10^{10} cm^{-2}, HEr (squares), alpha particle irradiation, Hal (circles) and EBD, He (triangles).

FIG. 10. Depth profiles of the major defect detected in p- $Si_{0.947}Ge_{0.053}$ after Er implantation, and e-beam deposition (no shielding the secondary electrons). The depth distribution of the vacancies and the Er ions (both derived from SRIM simulations) are also shown for comparison.

FIG. 11. (Color online) DLTS spectra for 3×10^{13} cm^{-2} 160 keV Er implanted $Si_{1-x}Ge_x$ (x = 0.053, 0.102 and 0.154). The spectra were recorded at a LIA frequency of 46 Hz. The inset depicts the DLTS spectra after 160 keV Er implanted $Si_{0.898}Ge_{0.102}$. Curves (a)-(c): DLTS spectrum of as-implanted $Si_{0.90}Ge_{0.10}$: Er (fluence = 3×10^{13} cm^{-2}), as implanted $Si_{0.898}Ge_{0.102}$: Er (fluence = 1×10^{10} cm^{-2}), after rapid thermal annealing at 850 ºC for 30 s of $Si_{0.898}Ge_{0.102}$: Er (fluence = 3×10^{13} cm^{-2}), respectively. DLTS spectra were recorded under identical DLTS conditions (reverse bias V_r = 1V, filling pulse V_p=1.6 V and a lock-in-amplifier frequency of 46 Hz).

Fig. 12. DLTS Arrhenius plot of defects in 160 keV Er implanted $Si_{1-x}Ge_x$ (x = 0.053, 0.102 and 0.154). Open circle and filled squares are for the defects detected after low fluence (LF:1×10^{10} cm^{-2}) and high fluence (HF: 3×10^{13} cm^{-2}) Er implantation, respectively.

FIG. 13. Photoluminescence spectra at room temperature of Er-implanted and annealed $Si_{1-x}Ge_x$: Er ($0 < x < 0.15$) (160 keV to a fluence of 3×10^{13} Er/cm^2). The samples were annealed in a rapid thermal processor at 850 ºC for 30 s.

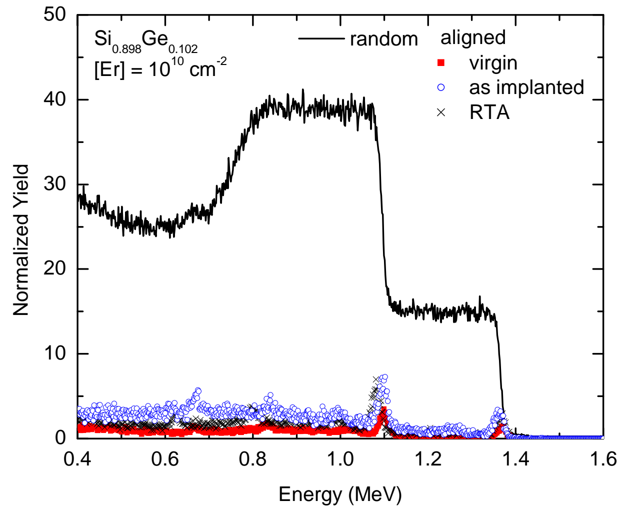

Fig1/13

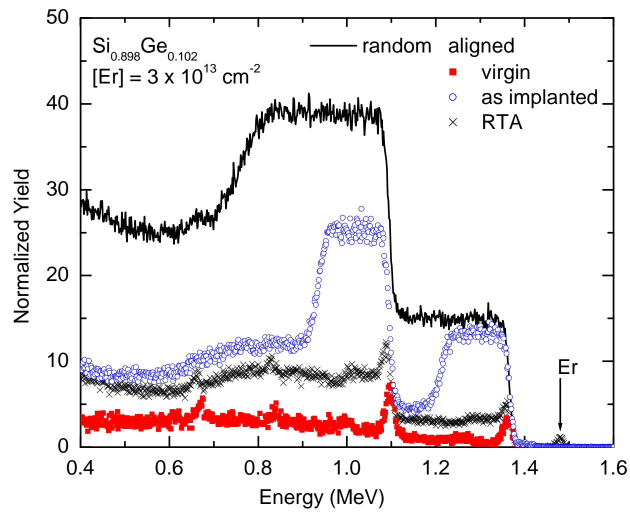

Fig2/13

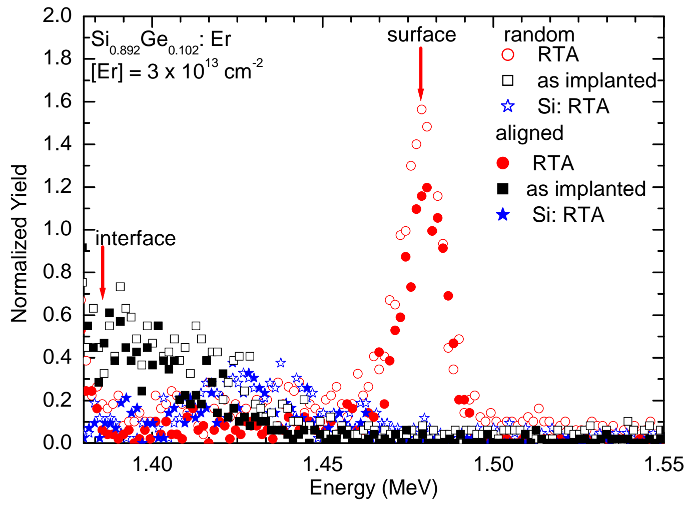

Fig3/13

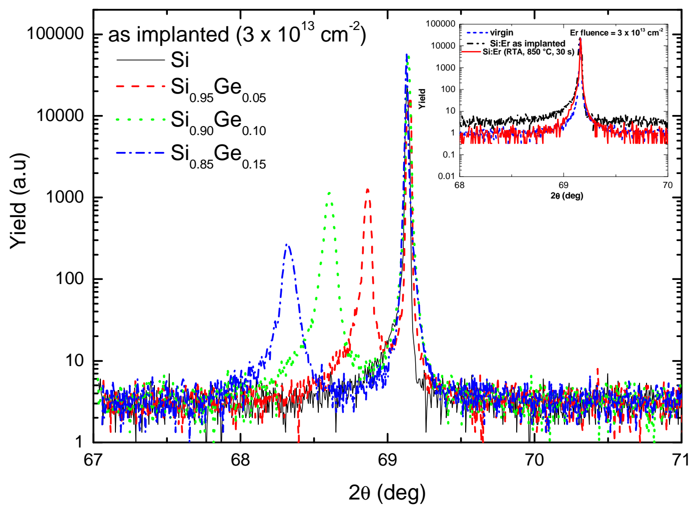

Fig4/13

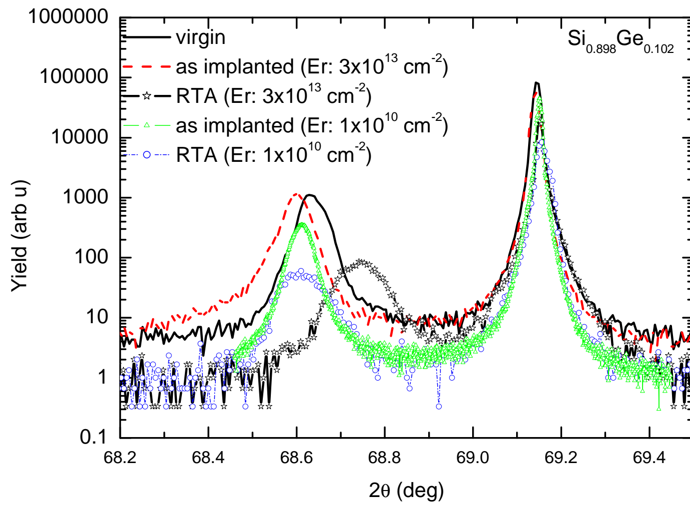

Fig5/13

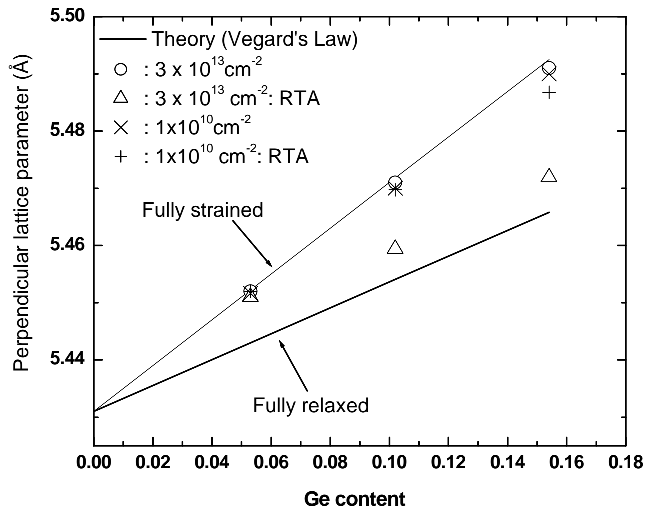

Fig6/13

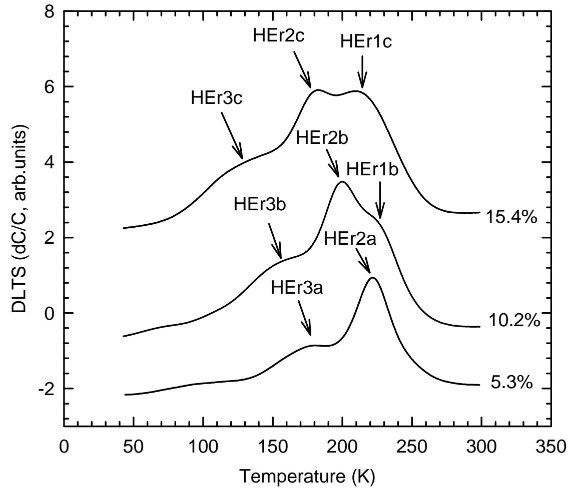

Fig7/13

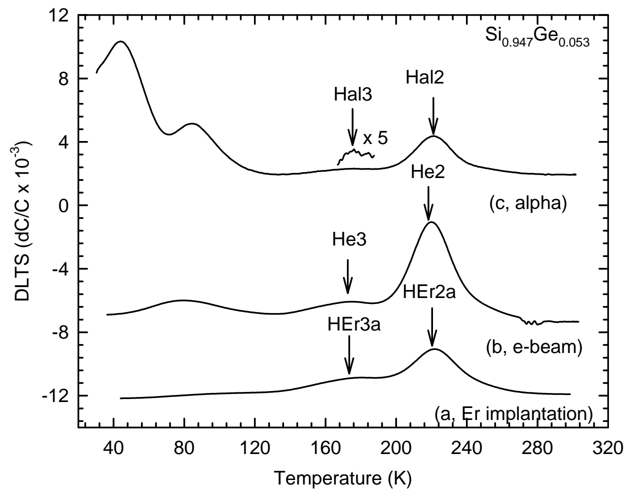

Fig8/13

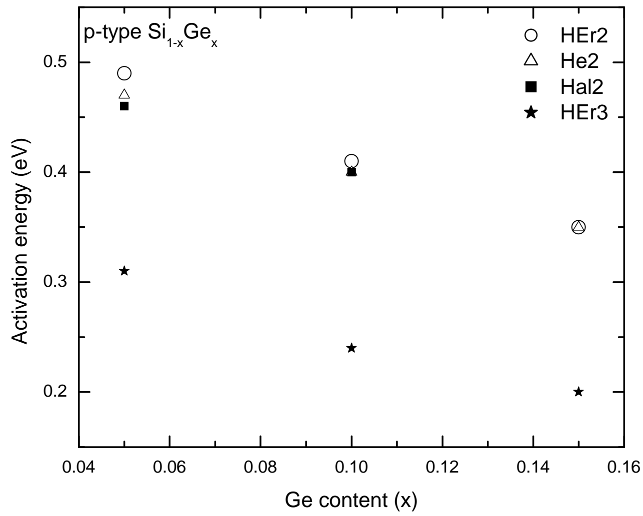

Fig9/13

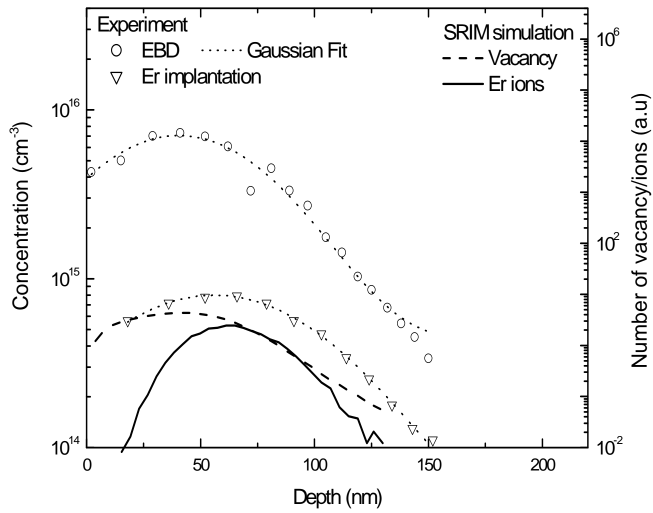

Fig 10/13

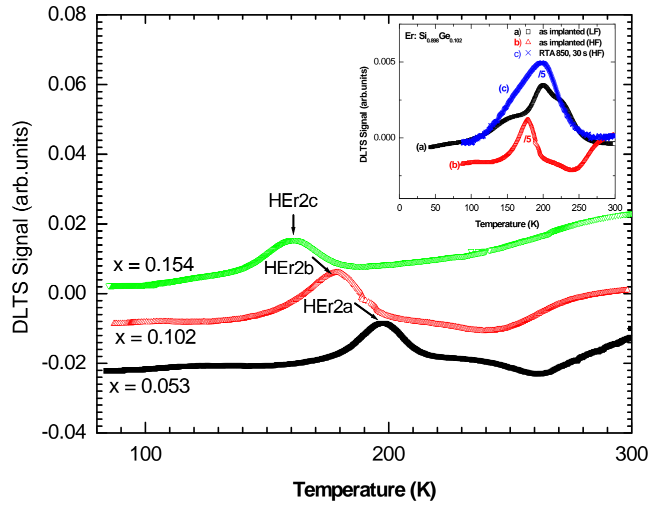

Fig11/13

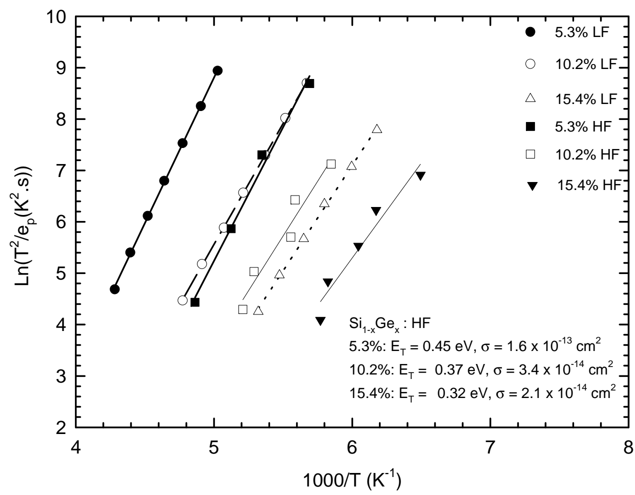

Fig12/13

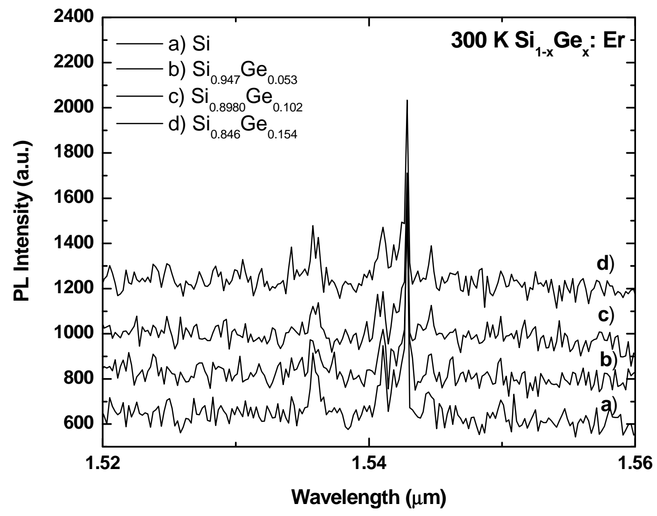

300 K $Si_{1-x}Ge_x$: Er
a) Si
b) $Si_{0.947}Ge_{0.053}$
c) $Si_{0.8980}Ge_{0.102}$
d) $Si_{0.846}Ge_{0.154}$
PL Intensity (a.u.)
Wavelength (μm)
d)
c)
b)
a)
2400
2200
2000
1800
1600
1400
1200
1000
800
600
1.52
1.54
1.56